Numerical studies on time-domain responses of on–off-keyed modulated optical signals through a dense fog

Urachada Ketprom, Yasuo Kuga, Sermsak Jaruwatanadilok, and Akira Ishimaru

We present a numerical technique to simulate the propagation characteristics of an on–off-keyed modulated optical signal through fog. The on–off-keyed modulated light (a square wave) is decomposed into a finite number of harmonic components, and a numerical solution for the vector radiative transfer equation is obtained for each harmonic that corresponds to the modulation frequency. With this method we study the distortion and the pulse spread in the received signal due to attenuation and scattering. We investigate the propagation characteristic of the modulated signal with different communication system parameters. This information can be used to study communication channel reliability. © 2004 Optical Society of America

OCIS codes: 030.5620, 060.4510, 290.1310.

1. Introduction

There is an increasing interest in free-space optics (FSO) communication systems among data service providers. The cost of installing a new fiber network in an urban environment is often expensive, and a less-expensive method is needed. A high-speed data link, for example, can be designed by either optical or millimeter-wave (MMW) point-to-point communication systems. The optical system is often the preferred method because of its simplicity and security. The data rate for short-distance FSO systems in an ideal condition can exceed 1 Gbit/s. However, both MMW and optical links are susceptible to adverse weather conditions. The presence of particulate matter creates attenuation and scattering. The amount of scattering is related to the size of the atmospheric particles with respect to the wavelength of a communication system, and it becomes substantial when particle size is comparable to or greater than the wavelength. In the case of the MMW link, the main problem is usually heavy rain. On the other hand, the main problem of the FSO link is usually fog, low clouds, smog, and dust. In cities such as San Francisco and Seattle, the presence of morning fog limits the highest data rate.

The traditional method to estimate the effects of an atmospheric channel is to calculate the attenuation characteristics based on the size distribution and concentration of particles along the signal path length. For a microwave link operating below 10 GHz, the scattering and attenuation by rain can be estimated with the Rayleigh approximation.[1,2] For a MMW link operating above 30 GHz, the Mie solution is commonly used to calculate scattering and absorption by rain.[1,2] For a FSO link, the Mie solution is also used to estimate loss due to fog and clouds. From the signal attenuation rate, the bit-error rate is usually estimated.[3] With this approach, however, we do not consider the propagation characteristics of modulated signals. The signal dispersion and eye-diagram distortion can be obtained only by means of studying the propagation of modulated signals. In addition, the signal dispersion is due to the multiple-scattering effects.[1,2,4] If the first-order single-scattering approximation is used for analysis, the signal dispersion of optical signals cannot be estimated. In this paper we give a numerical method to calculate the waveform of an intensity-modulated optical signal through a layer of fog and cloud. Our approach takes into account the multiple-scattering effects and reveals a substantial amount of waveform distortion.

The authors are with the Department of Electrical Engineering, P.O. Box 352550, University of Washington, Seattle, Washington 98195. The e-mail address for U. Ketprom is uketprom@u.washington.edu.

Received 14 April 2003; revised manuscript received 29 August 2003; accepted 26 September 2003.

0003-6935/04/020496-10$15.00/0

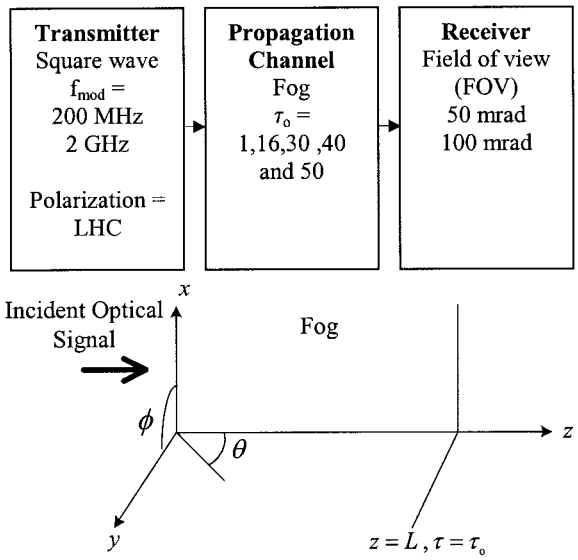

Fig. 1. Top: simulated optical communication system and propagation channel. LHC, left-hand circular. Bottom: plane-parallel problem and definitions.

2. Description of the Model

The majority of FSO communication systems are based on either 850- or 1550-nm wavelength laser systems, which have different power and distance characteristics. A simplified model of the FSO link is shown in Fig. 1. It is assumed that a laser ($\lambda = 0.8$ μm or $\lambda = 1.5$ μm) is used as a transmitter, and the on–off modulation frequencies f_{mod} are 200 MHz and 2 GHz. The on–off-keyed modulated signal (square wave) is modeled by a Fourier series expansion with the fundamental, third, fifth, seventh, and ninth harmonics of the modulation frequency. We assume that the transmitted light has a left-hand circular polarization. The fog is modeled by a uniform layer of randomly distributed water particles with a size distribution shown in Table 1. The refractive index of a fog particle is $n_{\mathrm{fog}} = 1.3289 + i0.0013289$ at $\lambda = 0.8$ μm and $1.319 + i0.001319$ at $\lambda = 1.5$ μm. The fog layer (path length) is assumed to be $L = 1$ km, and the concentration of fog particles is varied according to the optical depth τ_0 defined by $\tau_0 = \rho\sigma_t L$ where ρ is the number density (number of particles per unit volume, m^{-3}) and σ_t is the total scattering cross section of a single particle (m^{-2}). The scattering and

Table 1. Particle Size Distribution of the Fog

Diameter of Particle (μm)	Number of Particles per Cubic Centimeter
0.4	3
0.6	10
0.7	40
1.4	50
2.0	7
3.6	1
5.4	9
8.0	2

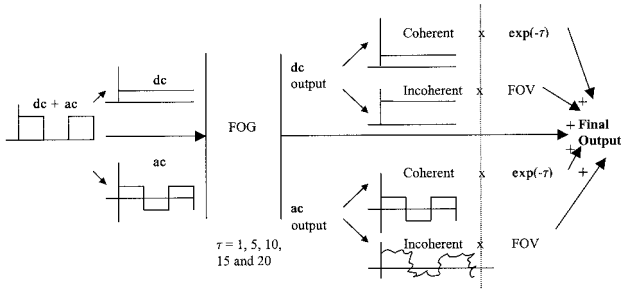

Fig. 2. Block diagram of numerical simulations.

attenuation by a single particle is obtained by the Mie solution. The transmitted intensity as a function of angle is calculated by the numerical solutions of the vector radiative transfer (RT) equation.[5] The receiver has a finite field of view (FOV), and the received intensity must be obtained by integration over the receiver FOV. By summing the average (dc) and harmonic components, we can estimate the time-domain responses of the on–off-keyed modulated signal. The waveform of the received signal is strongly dependent on the receiver FOV. A narrow FOV reduces the amount of multiple-scattered light, and the received waveform will be close to that of the transmitted signal. The disadvantage is that the small-FOV receiver collects fewer photons, which may limit the signal-to-noise ratio in a heavy fog. A wide-FOV receiver collects more photons, which may be advantageous in a heavy fog. However, some of these photons will be multiple scattered, which may cause waveform distortion.

The main task is to develop a method that can simulate the propagation channel shown in Fig. 1, including multiple-scattering effects. For a plane wave incident on a homogeneous layer of particles, the most accurate results can be obtained with the numerical solution of the vector RT equation.[2,5] Recently, we developed a technique to include the envelope-modulated light or photon density wave in the RT equation.[6] We will apply this new method for analyzing communication channels. To simulate the propagation characteristics of the on–off-keyed modulated signal, we need to calculate four different cases as shown in Fig. 2. The on–off-keyed modulated light is separated into the average (dc) and modulated (ac) signals. Both dc and ac signals can be separated into the coherent (reduced incident light) and incoherent (scattered) light. Each is calculated separately by the RT equation. As shown in Fig. 2, the received signal consists of four intensities. The incident light is assumed to be a plane wave, and the FOV of the receiver has no effect on the coherent (unscattered) signal. However, the scattered light arrives from different angles, and the total incoherent intensity is given by the integration of the specific intensity over the receiver FOV.

3. Formulation with the Radiative Transfer Equation

As shown in Fig. 2, the reduced incident (coherent) light is simply given by the exponential decay. How-

ever, to obtain the incoherent light, the RT equation must be solved. Consider a plane wave propagating through a slab of a random medium of thickness L in a plane-parallel medium over the optical distance τ defined by $\tau = \rho\sigma_t z$ where ρ is the number density, σ_t is the total scattering of a single particle, and z is the actual distance. The random medium is defined as randomly located dielectric spheres suspended in a homogeneous background. It is common to formulate the RT equation with the modified Stokes vector. The specific intensity I written in the form of the modified Stokes vector is[2,5]

$$I = [I_1 I_2 UV]^T = [\langle E_1 E_1^* \rangle \langle E_2 E_2^* \rangle 2\ \mathrm{Re} \times \langle E_1 E_2^* \rangle 2\ \mathrm{Im} \langle E_1 E_2^* \rangle]^T, \quad (1)$$

where E_1 and E_2 are vertically and horizontally polarized electric fields, * denotes complex conjugate, and T is the transpose operator of a matrix. The time-dependent modified RT equation that solves for the modified Stokes vector through a random medium is expressed as[1,2]

$$\left(\mu \frac{\partial}{\partial \tau} + 1 + \frac{1}{\tau_0}\frac{\partial}{\partial t_n}\right) I(t_n, \tau, \mu, \phi) = \int_0^{2\pi}\int_{-1}^{1} S(\mu, \phi, \mu', \phi')[I(t_n, \tau, \mu', \phi')]\mathrm{d}\mu'\mathrm{d}\phi' + J(t_n, \tau, \mu, \phi), \qquad \text{for } 0 \le \tau \le \tau_0. \quad (2)$$

τ_0 is the optical depth defined by $\tau_0 = \rho\sigma_t L$ where L is the length of the slab of the random medium. The coordinate system is defined in Fig. 1. The normalized time $t_n = t\,(L/c)^{-1}$ where c is the speed of the wave in the medium. $[I] = 4 \times 1$ specific intensity, $[S] = 4 \times 4$ scattering matrix, J is the source term, and $\mu = \cos\theta$ is the cosine of the polar angle. The scattering matrix is expressed in terms of the scattering amplitude f_{11}, f_{12}, f_{21}, and f_{22} and is calculated by Mie theory and explained in detail by Cheung and Ishimaru.[5]

$$[S] = \frac{1}{\rho\sigma_t}\begin{bmatrix} \rho|f_{11}|^2 & \rho|f_{12}|^2 & \rho\ \mathrm{Re}(f_{11}f_{12}^*) & -\rho\ \mathrm{Im}(f_{11}f_{12}^*) \\ \rho|f_{21}|^2 & \rho|f_{22}|^2 & \rho\ \mathrm{Re}(f_{21}f_{22}^*) & -\rho\ \mathrm{Im}(f_{21}f_{22}^*) \\ \rho 2\ \mathrm{Re}(f_{11}f_{21}^*) & \rho 2\ \mathrm{Re}(f_{12}f_{22}^*) & \rho\ \mathrm{Re}(f_{11}f_{22}^* + f_{12}f_{21}^*) & -\rho\ \mathrm{Im}(f_{11}f_{22}^* - f_{12}f_{21}^*) \\ \rho 2\ \mathrm{Im}(f_{11}f_{21}^*) & \rho 2\ \mathrm{Im}(f_{12}f_{22}^*) & \rho\ \mathrm{Im}(f_{11}f_{22}^* + f_{12}f_{21}^*) & \rho\ \mathrm{Re}(f_{11}f_{22}^* - f_{12}f_{21}^*) \end{bmatrix}. \quad (3)$$

The specific intensity I in Eq. (1) consists of the constant (dc in Fig. 2) term and the time-dependent (ac in Fig. 2) term, i.e.,

$$I_{\mathrm{total}}(t) = I_{\mathrm{constant}} + I(t)\exp(-i\omega_{\mathrm{mod}}t), \quad (4)$$

where $\omega_{\mathrm{mod}} = 2\pi f_{\mathrm{mod}}$ and f_{mod} is the modulation frequency. The specific intensity through random media is separated into two parts: the reduced intensity (coherent) and the diffused intensity (incoherent) and are calculated separately. Therefore we can rewrite Eq. (4) such that

$$I_{\mathrm{total}}(t) = I_{\mathrm{total\_reduced}}(t) + I_{\mathrm{total\_diffused}}(t). \quad (5)$$

We further separate the constant (dc) term and time-dependent (ac) term as shown in Fig. 2.

$$I_{\mathrm{total\_reduced}}(t) = I_{\mathrm{ri\_dc}} + I_{\mathrm{ri\_ac}}, \quad (6)$$

$$I_{\mathrm{total\_diffused}}(t) = I_{d\_\mathrm{dc}} + I_{d\_\mathrm{ac}}, \quad (7)$$

$$I_{\mathrm{total}}(t) = I_{d\_\mathrm{dc}} + I_{d\_\mathrm{ac}} + I_{\mathrm{ri\_dc}} + I_{\mathrm{ri\_ac}}, \quad (8)$$

where $L_{\mathrm{ri\_dc}}$ is the reduced intensity of the constant term and $I_{\mathrm{ri\_ac}}$ is the reduced intensity of the time-dependent term. Similarly, the diffused intensity I_d consists of both constant and time-dependent terms. The reduced intensity decreases exponentially because of scattering and absorption by particles, and it satisfies the equation

$$\frac{\partial}{\partial \tau} I_{\mathrm{ri}} = -I_{\mathrm{ri}}, \quad (9)$$

where I_{ri} is the reduced intensity (coherent). I_{ri} is expressed as

$$I_{\mathrm{ri}}(t, \tau) = I_0 f(t, \tau)\exp(-\tau)\delta(\mu - 1)\delta(\phi), \quad (10)$$

where I_0 is the incident modified Stokes vector. In this paper left-handed circular polarization is used.

$$I_0 = [1/2\ 1/2\ 0\ 1]^T, \quad (11)$$

where $f(t, \tau)$ is the pulse-shape function and it is defined as

$$f(t, \tau) = \exp\left[-i\omega_m\left(t - \frac{\tau}{\tau_0}\right)\right], \quad (12)$$

where $\omega_m = \omega_{\mathrm{mod}}(L/c)$ is the normalized angular modulation frequency. The unmodulated (dc) light is given when we set $\omega_m = 0$. The diffused intensity satisfies Eq. (2) and can be expressed as

$$\left(\mu \frac{\partial}{\partial \tau} + 1 + \frac{1}{\tau_0}\frac{\partial}{\partial t_n}\right) I_d(t_n, \tau, \mu, \phi) = \int_0^{2\pi}\int_{-1}^{1} S(\mu, \phi, \mu', \phi')[I_d(t_n, \tau, \mu', \phi')]\mathrm{d}\mu'\mathrm{d}\phi' + E_{\mathrm{ri}}(t_n, \tau, \mu, \phi), \qquad \text{for } 0 \le \tau \le \tau_0. \quad (13)$$

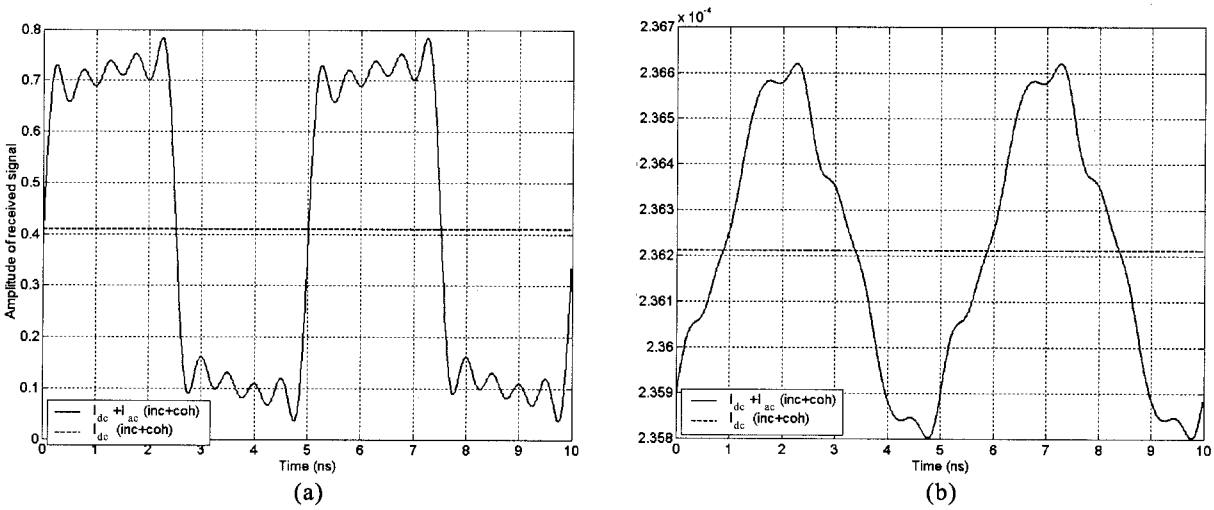

Fig. 3. Received (ac plus dc) signal waveforms of 0.8-μm wavelength and 200-MHz modulation frequency with a FOV of 50 mrad for (a) $\text{tau}_0 = 1$, (b) $\text{tau}_0 = 16$.

Because there is no source in a fog layer, the source term J in Eq. (2) has only the contribution from the incident wave. Thus we can replace source term J with the equivalent source term E_{ri}, which is defined as

$$E_{\text{ri}} = \int_0^{2\pi} \int_{-1}^{1} S(\mu, \phi, \mu', \phi') I_{\text{ri}}(t, \tau, \mu', \phi') \mathrm{d}\mu' \mathrm{d}\phi' = F_0(\mu, \phi) f(t, \tau) \exp(-\tau), \tag{14}$$

where $F_0 = S(\mu, \phi, 1, 0) I_0$ and the pulse-shape function $f(t, \tau)$ is the same as in Eq. (12). The diffused intensity is created inside a fog layer and there is no diffuse intensity entering from outside. These boundary conditions are given as

$$I_d'(\tau = 0) = 0 \qquad \text{for } 0 \le \mu \le 1, \tag{15}$$

$$I_d'(\tau = 0) = 0 \qquad \text{for } -1 \le \mu \le 0. \tag{16}$$

Although Eqs. (2), (10), and (13) are expressed in the time domain, the actual numerical solution for the RT equation is obtained in the frequency domain.[5,6] The time-domain response is usually simulated when we take a Fourier transform of the band-limited frequency-domain results. In the frequency domain, Eq. (13) can be expressed as

$$\mu \frac{\partial}{\partial \tau} I_d'(\omega', \tau, \mu) \left[1 + (\mu - 1) i \frac{\omega' + \omega_m}{\tau_0} \right] I_d'(\omega, \tau, \mu) = \int_0^{2\pi} \int_{-1}^{1} S(\mu, \phi, \mu', \phi') I_d'(\omega', \tau, \mu', \phi') \mathrm{d}\mu' \mathrm{d}\phi' + F_0(\mu, \phi) f(\omega', \tau) \exp(-\tau), \tag{17}$$

where $\omega = \omega_m + \omega'$, with ω the normalized angular frequency and ω_m the normalized angular modulation frequency. We also use $I_d'(\omega, \tau) = I_d(\omega, \tau)\exp(-i\omega\tau/\tau_0)$ to avoid numerical instability.[6] The pulse-shape function $f(\omega', \tau)$ for a sinusoidal signal is given by

$$f(\omega', \tau) = 2\pi\delta(\omega'). \tag{18}$$

The constant or dc term is given when we set $\omega_m = 0$. To solve for the on–off-keyed modulated time-dependent term, first we need to estimate the required number of harmonic components that corresponds to ω_m. In our simulations, we used the fundamental, third, fifth, seventh, and ninth harmonics. Because our method is based on the Fourier series expansion of the modulated signal, the input must be a periodic signal. Equation (17) is solved numerically by the discrete ordinate Gauss quadrature method.[2,5]

4. Results and Discussion

We conducted numerical simulations for both 0.8- and 1.5-μm wavelengths using the size distribution shown in Table 1. The average particle size is 1.536 μm with a standard deviation of 0.7247 μm. The results for a modulation frequency of 200 MHz for both 0.8- and 1.5-μm wavelengths are shown in Figs. 4, 6, and 11. The results of 2 GHz for the 1.5-μm wavelength are dominated by the coherent intensity and do not show any waveform distortion. Therefore all results of $f_{\text{mod}} = 2$ GHz are for the 0.8-μm wavelength only. To show a significant waveform distortion at 1.5 μm, the average particle size must be much larger than that of Table 1.

The results are divided into three main parts. The first part shows the result of the 0.8-μm wavelength and a modulation frequency of a 200-MHz system, the effects of FOV and optical depth, and the eye diagrams. The second part compares the modulation frequency of 200 MHz and 2 GHz for the 0.8-μm wavelength system. The third part explains the effect of different wavelengths, 0.8 and 1.5 μm, for the same modulation frequency of 200 MHz.

The total received signal (dc plus ac) results are

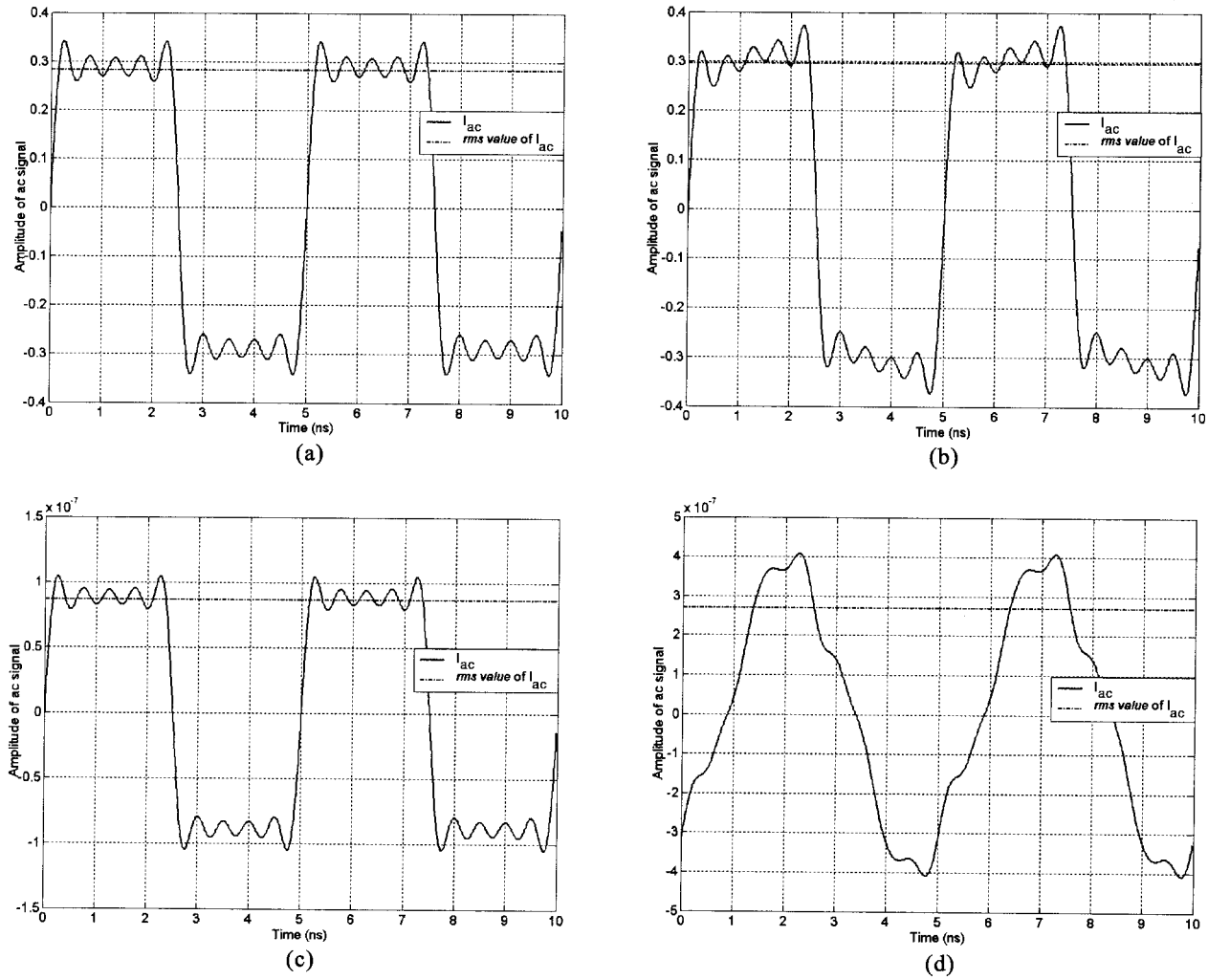

Fig. 4. Received ac signal waveforms of 0.8-μm wavelength and 200-MHz modulation frequency for (a) $\tau_0 = 1$, FOV of 1 mrad; (b) $\tau_0 = 1$, FOV of 50 mrad; $\tau_0 = 16$, FOV of 1 mrad; (d) $\tau_0 = 16$, FOV of 50 mrad.

shown in Fig. 3. The dashed lines in Figs. 3(a) and 3(b) represent the dc value. At higher optical depths, the dc component will dominate the ac component, and thus it is difficult to show the result with the dc value added. The distortion is more apparent with only the ac component at high optical depth. Thus we consider only the ac component for the result.

A. 0.8-μm Carrier Wavelength at 200-MHz Modulation Frequency

1. Effect of Field of View

The time-domain responses of the copolarized intensity (left-handed circular polarization) for two different FOVs at a modulation frequency of 200 MHz and at two optical depths $\tau_0 = 1$ and 16 are shown in Fig. 4. When the optical distance and FOV are small such as $\tau_0 = 1$ and a FOV of 1 mrad, the received signal is mostly the reduced incident intensity, and the contribution of scattered intensity is negligible. The received waveform is almost the same as the original shape in Fig. 4(a). Increasing the FOV to 50 mrad while fixing $\tau_0 = 1$, we generate the same result in Fig. 4(b) because the scattered intensity for such a small optical depth $\tau_0 = 1$ is small compared with the reduced intensity. Therefore the received signal is dominated by the reduced incident intensity.

The FOV effect is obvious when optical depth is as high as $\tau_0 = 16$ and at the wider FOV of 50 mrad. Both the reduced incident and the scattered intensities can be detected, and the total intensity is approximately four times the value of the case of a FOV of 1 mrad. The waveform in Fig. 4(d) ($\tau_0 = 16$ and a FOV of 50 mrad) shows the distortion effect caused by the scattered intensity that is not visible in Fig. 4(c) ($\tau_0 = 16$ and a FOV of 1 mrad) because the narrow FOV rejects the scattered intensity. Because our method is based on the Fourier series expansion of the on–off-keyed modulated signal and only five harmonic components are used, the received signal is not a perfect square wave. Nevertheless the waveform distortion can be seen in the simulated results.

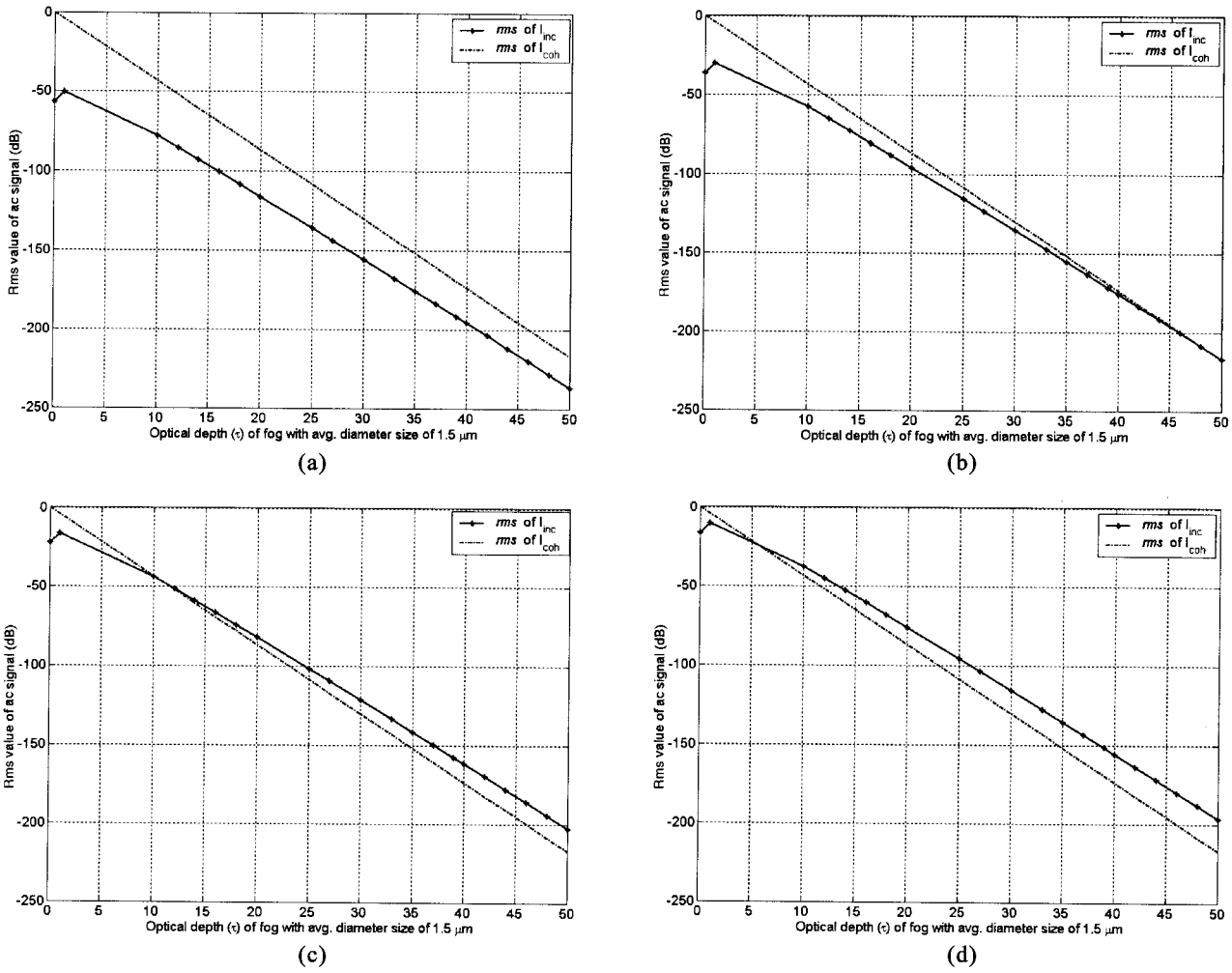

Fig. 5. rms values of incoherent and coherent intensity of 0.8-μm wavelength and 200-MHz modulation frequency versus τ_0 for (a) FOV of 1 mrad, (b) FOV of 10 mrad, (c) FOV of 50 mrad, (d) FOV of 100 mrad.

2. Incoherent Intensity versus Coherent Intensity

The average (dc) intensity of the incident signal is 0.9357 W/m^2 whereas the rms value of the incident modulated signal (ac) is 0.701 W/m^2. The rms value of the ac signal is shown as dashed–dotted lines in Figs. 4(a)–4(d). Both the average and modulated intensities decrease as the optical distance increases for the limited FOV.

The rms value of the ac signal contains both rms values for reduced (coherent) and scattered intensity (incoherent). These two rms values are shown in Fig. 5 as a function of an optical depth. Coherent intensity does not depend on the FOV, and its decreasing rate depends on a function $\exp(-\tau_0)$. A wide FOV allows more incoherent intensity to contribute to the received waveform. The incoherent intensity carries the scattering effect that results in distortion and pulse spread in the waveform. Therefore, when the incoherent intensity becomes dominant, distortion and pulse spread occur. In general, the waveform distortion starts to occur when the rms values of coherent and incoherent intensities become comparable, and the distortion becomes worse as optical depth increases.

For the current system of an 0.8-μm carrier wavelength at 200-MHz modulation frequency, the incoherent intensity starts to dominate the coherent intensity approximately at $\tau_0 = 12$ for a FOV of 50 mrad. The resulting distorted waveform for $\tau_0 = 16$ after the domination of the incoherent intensity can be seen in Fig. 4(d).

3. Effect of Optical Depth

At high optical depth, the received signal is severely distorted. The received signal is mostly the incoherent intensity. The distortion is measured by the waveform's shape, amplitude, and phase. For $\tau_0 = 16$, the waveform shape is no longer a square wave, the amplitude is much less than the transmitted wave, and the phase shift causes a pulse spread effect. The phase shift can easily be seen when the optical depth is as high as $\tau_0 = 30$ or 40 as shown in Fig. 6. The received signal in Fig. 6 has a phase shift greater than 180° and a pulse spread that causes an

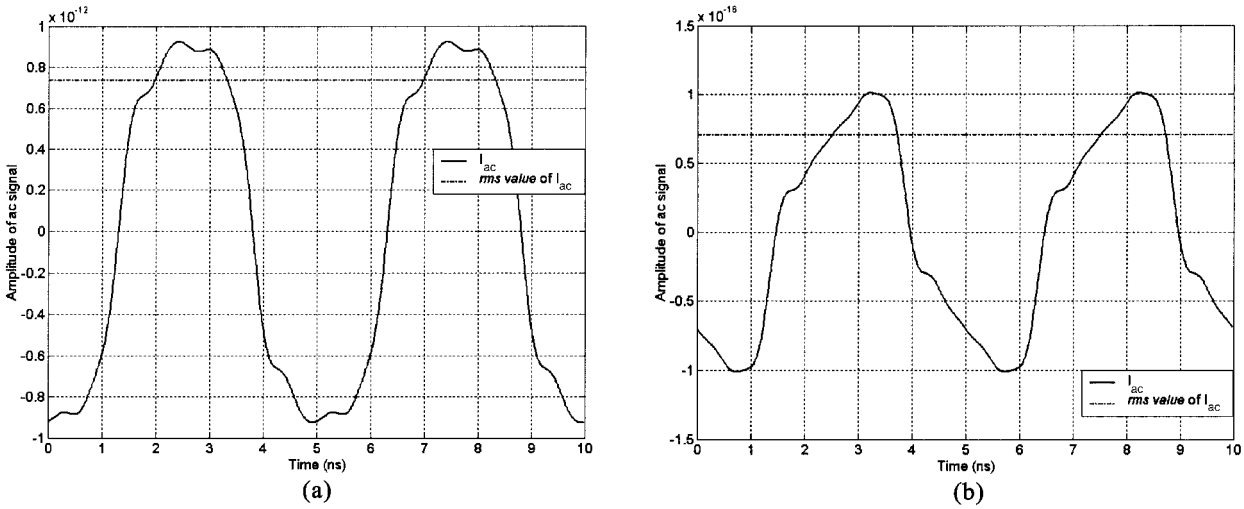

Fig. 6. ac signal waveforms of 0.8-μm wavelength and 200-MHz modulation frequency with a FOV of 50 mrad for (a) $\tau_0 = 30$ and (b) $\tau_0 = 40$.

error in transmitting. The distortion and pulse spread will result in a bit error in transmission.

The eye diagram is commonly used to evaluate digital communication channels.[7] A wide and stable eye means that the digital signal can be recovered accurately from the received signal. A distorted eye or closed eye shows potential problems. To obtain the eye diagram, the incident intensity without fog is used as a reference signal, and the received intensity is plotted over one period. Because a pseudo-square wave is used in our study, the shape of eye is not that of a sinusoidal signal or a square wave. Figure 7 shows the eye diagrams for different values of τ_0 for a FOV of 50 mrad. When the FOV is small, such as a FOV of 1 mrad, the received signal is mostly coherent intensity, and the eye diagram does not change as τ_0 increases. However, the signal-to-noise ratio that is usually limited by the receiver noise, decreases rapidly as τ_0 increases. For a wide FOV, such as a FOV of 50 mrad, a significant distortion can be seen in the eye diagram. If the data sample time is fixed for a coherent intensity, this may create a high bit-error rate. However, when the data sample point is changed, it seems that the original data can be recovered correctly.

B. 0.8-μm Carrier Wavelength at 2-GHz Modulation Frequency

The effect of a different modulation frequency can be seen when we compare two modulated frequencies, 200 MHz and 2 GHz, for the 0.8-μm carrier wavelength. Figure 8 shows that, at 2 GHz, the incoherent intensity is substantially dominant when $\tau_0 > 35$, and the received ac signal in Fig. 9(d) shows the severe distortion accordingly. Because a random medium acts as a low-pass filter to the transmitted optical signal, the incoherent intensity at a higher frequency will be less. The amplitude of the received signal at 2 GHz is approximately four times smaller than at 200 MHz compared between Fig. 9(c) and Fig. 6(a) because, at high optical depth, the received signal is mainly composed of the incoherent intensity. The received signal of 2 GHz in Fig. 9(d) is less distorted because the incoherent intensity does not dominate the coherent intensity as much as the received signal of 200 MHz in Fig. 6(b).

C. 1.5-μm Carrier Wavelength at 200-MHz Modulation Frequency

Next, the results of a different carrier wavelength, 1.5 μm with a 200-MHz modulated frequency, and the same FOV and optical depth used in previous results are shown for comparison. Figure 10(a) shows that the incoherent intensity is obviously dominant when $\tau_0 > 30$, which is higher than the results of the 0.8-μm system at $\tau_0 > 20$ in Fig. 5(c). This information suggests that 1.5 μm contains less scattering intensity information than the 0.8-μm system for the same parameters in FOV, optical depth, and modulated frequency. Thus the result in Fig. 11(d) is not as distorted as Fig. 6(b) for the highest simulated value of optical depth. For 2 GHz, the distortion will not appear for $\tau_0 < 50$ because the incoherent intensity does not dominate the coherent intensity that can be seen in Fig. 10(b). The result in Fig. 11 shows the received signal waveform for different optical depths before and after the incoherent intensity becomes dominant for the 200-MHz modulation frequency and the 1.5-μm wavelength system.

5. Conclusions

We have developed a numerical method to evaluate the propagation characteristics of modulated optical signals through fog or clouds. Unlike the traditional cw signal attenuation technique that has been used to estimate the bit-error rate, with our method we directly calculate the waveforms of the modulated signal. The results displayed in the eye diagram

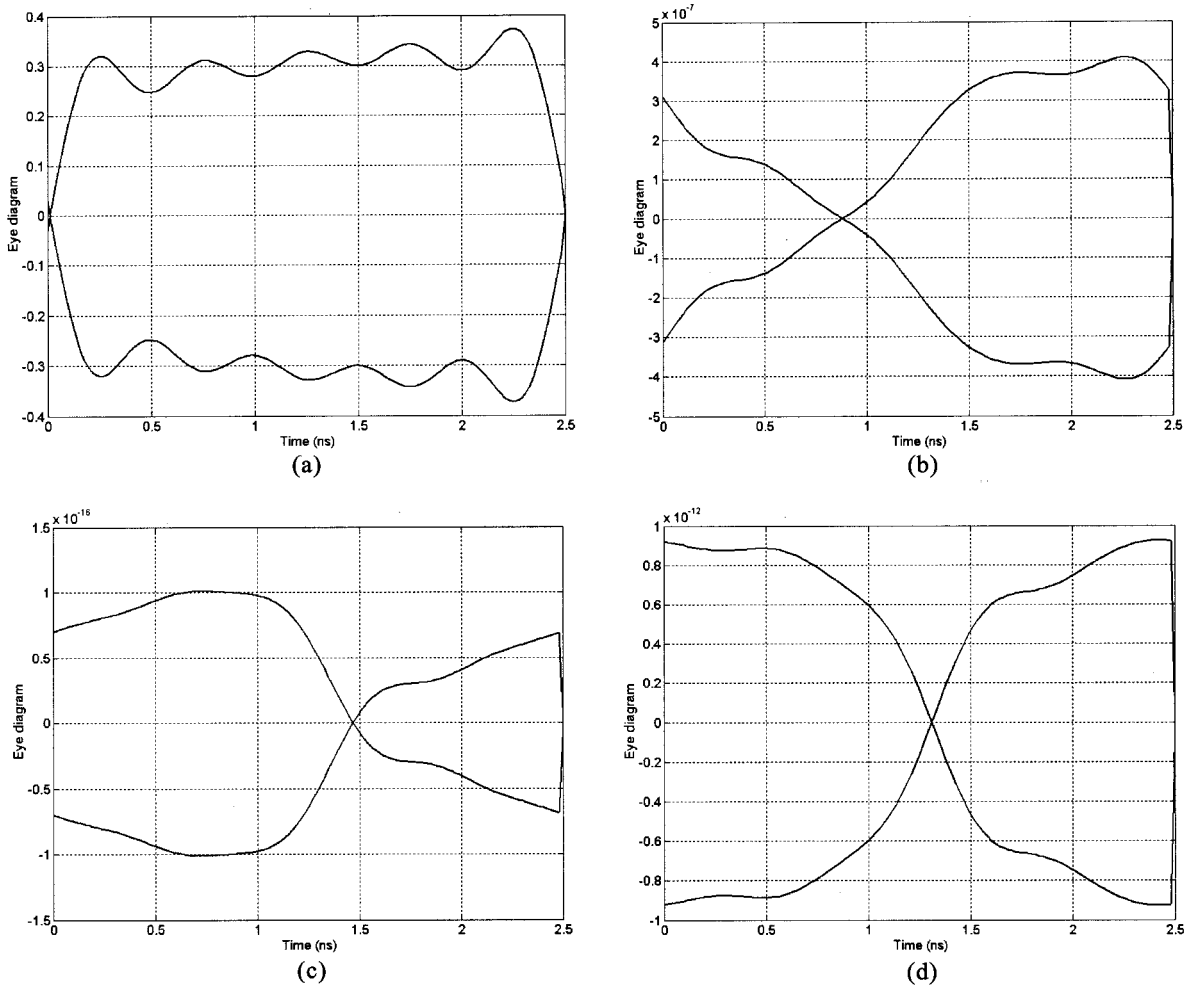

Fig. 7. Eye diagram: received waveforms of 0.8-μm wavelength and 200-MHz modulation frequency with a FOV of 50 mrad for (a) $\tau_0 = 1$, (b) $\tau_0 = 16$, (c) $\tau_0 = 30$, (d) $\tau_0 = 40$.

reveal that the data must be sampled at different times if the propagation channel is highly dispersive. Although a small FOV is useful to eliminate unwanted scattered light and to maintain an original waveform, the channel loss in a heavy fog can be substantial because of the exponential decay of the coherent intensity. This may result in loss of the communication link. In a heavy fog, the FSO system can be designed to take advantage of incoherent or scattered light. Although a signal from a wide-FOV receiver in a heavy fog will have a significant amount of waveform distortion, the signal-to-noise ratio is much better than that of the small-FOV case. It seems that it is still possible to maintain a high data rate if sampling occurs at a correct time. Our numerical method will provide the expected pulse delay and waveform distortion for a given fog condition, and it can be used in conjunction with the available timing-correction method including the proposed delayed diversity technique[3] that has shown to improve the bit-error rate of the FSO link in the presence of fog. The results shown in this paper are based on a fog size distribution that has an average diameter of 1.536 μm (Table 1). In our simulations, the waveform distortion at the 1.5-μm wavelength was small for a data transmission of 2 GHz. However, it is known that the average size of atmospheric particles can be much higher or the size distribution

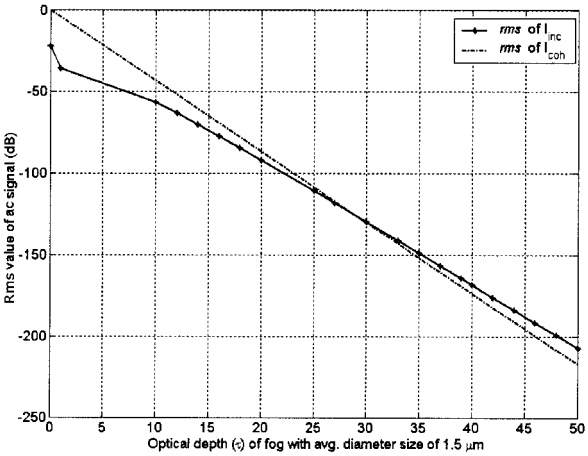

Fig. 8. rms values of incoherent and coherent intensity of 0.8-μm wavelength and 2-GHz modulation frequency with a FOV of 50 mrad versus τ_0.

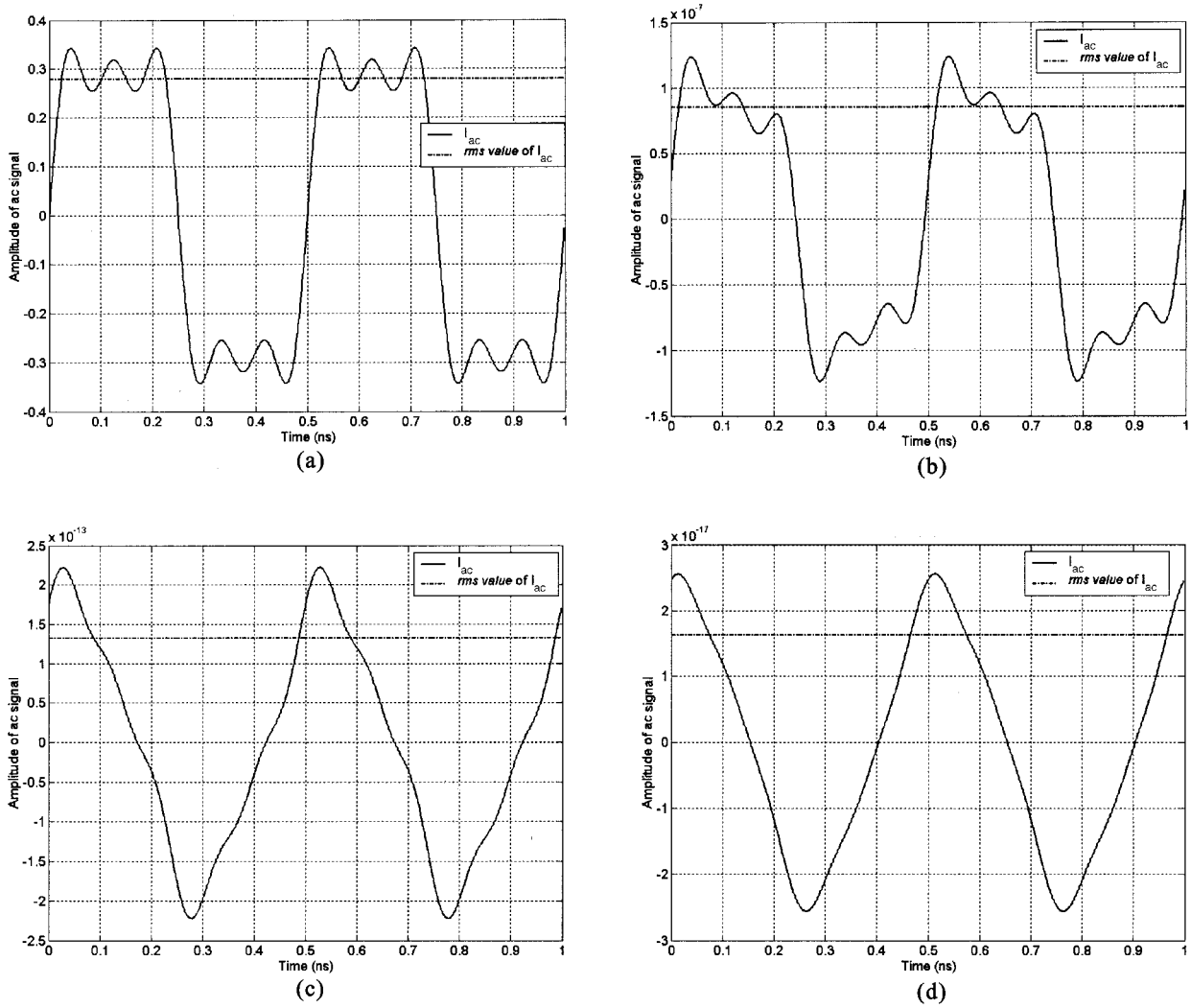

Fig. 9. Received ac signal waveforms of 0.8-μm wavelength and 2-GHz modulation frequency with a FOV of 50 mrad for (a) $\tau_0 = 1$, (b) $\tau_0 = 16$, (c) $\tau_0 = 30$, (d) $\tau_0 = 40$.

can contain a significant amount of large particles. Because the scattering increases dramatically as particle size becomes greater than the wavelength, we should expect that a communication link based on 1550-nm wavelength is equally susceptible to the waveform distortion due to fog and cloud. The

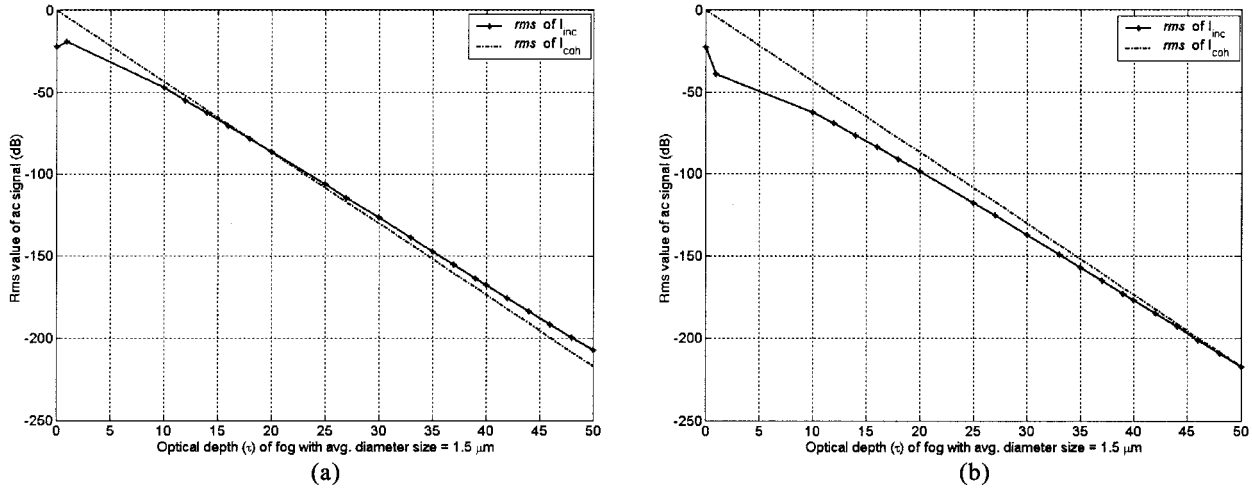

Fig. 10. rms values of incoherent and coherent intensity of 1.5-μm wavelength with a FOV of 50 mrad versus τ_0 for (a) frequency of 200 MHz, (b) frequency of 2 GHz.

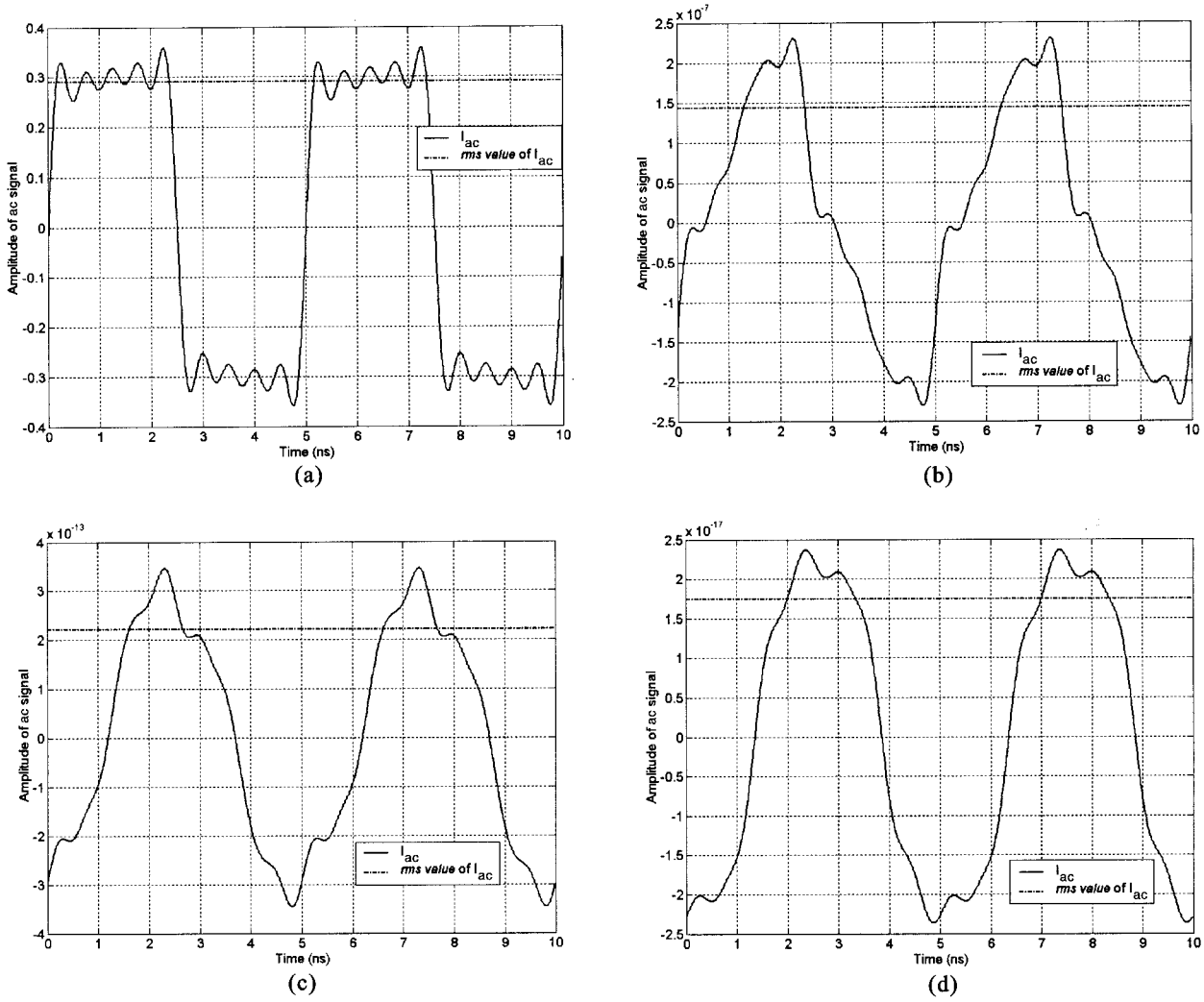

Fig. 11 Received ac signal waveforms of 1.5-μm wavelength and 2-GHz modulation frequency with a FOV of 50 mrad for (a) $\tau_0 = 1$, (b) $\tau_0 = 16$, (c) $\tau_0 = 30$, (d) $\tau_0 = 40$.

present method is limited to an intensity-modulated signal such as on–off keyed, and it cannot be used for a phase-modulated signal that is commonly used for a microwave and MMW communication link.

This research is supported by the National Science Foundation (ECS-9908849) and a Thai government scholarship (National Electronics and Computer Technology Center).

References

1. A. Ishimaru, S. Jaruwatanadilok, and Y. Kuga, "Polarized pulse waves in random discrete scatterers," Appl. Opt. **40,** 5495–5502 (2001).
2. A. Ishimaru, *Wave Propagation and Scattering in Random Media* (Institute of Electrical and Electronics Engineers, Piscataway, N.J., 1997).
3. C. Davis and I. Smolyaninov, "The effect of atmospheric turbulence on bit-error rate in an on-off-keyed optical wireless system," in *Free-Space Laser Communication and Laser Imaging*, D. G. Voelz and J. C. Ricklin, eds., Proc. SPIE **4489,** 129–131 (2002).
4. H. C. van de Hulst, *Multiple Light Scattering*, (Academic, New York, 1980), Vols. 1 and 2.
5. R. L. Cheung and A. Ishimaru, "Transmission, backscattering, and depolarization of waves in randomly distributed spherical particles," Appl. Opt. **21,** 3792–3798 (1982).
6. S. Jaruwatanadilok, A. Ishimaru, and Y. Kuga, "Photon density wave for imaging through random media," Waves Random Media **12,** 351–364 (2002).
7. L. W. Couch, *Modern Communication Systems* (Prentice-Hall, Englewood Cliffs, N.J., 1995).